

ELM-FBPINNs: An Efficient Multilevel Random Feature Method

Samuel Anderson¹, Victorita Dolean^{2*†}, Ben Moseley^{3†},
Jennifer Pestana^{1†}

¹*Department of Mathematics and Statistics, University of Strathclyde,
Glasgow, G1 1XH, UK.

²Department of Mathematics and Computer Science, Eindhoven
University of Technology, Eindhoven, 5600 MB, The Netherlands.

³Department of Earth Science and Engineering, Imperial College
London, London, SW7 2AZ, UK.

*Corresponding author(s). E-mail(s): v.dolean.maini@tue.nl;

Contributing authors: sam.anderson@strath.ac.uk;

b.moseley@imperial.ac.uk; jennifer.pestana@strath.ac.uk;

[†]These authors contributed equally to this work.

Abstract

Domain-decomposed variants of physics-informed neural networks (PINNs) such as finite basis PINNs (FBPINNs) mitigate some of PINNs' issues like slow convergence and spectral bias through localisation, but still rely on iterative non-linear optimisation within each subdomain. In this work, we propose a hybrid approach that combines multilevel domain decomposition and partition-of-unity constructions with random feature models, yielding a method referred to as multilevel ELM-FBPINN. By replacing trainable subdomain networks with extreme learning machines, the resulting formulation eliminates backpropagation entirely and reduces training to a structured linear least-squares problem. We provide a systematic numerical study comparing ELM-FBPINNs and multilevel ELM-FBPINNs with standard PINNs and FBPINNs on representative benchmark problems, demonstrating that ELM-FBPINNs and multilevel ELM-FBPINNs achieve competitive accuracy while significantly accelerating convergence and improving robustness with respect to architectural and optimisation parameters. Through ablation studies, we further clarify the distinct roles of domain decomposition and random feature enrichment in controlling expressivity, conditioning, and scalability.

Keywords: Domain decomposition; Physics-informed neural networks; Extreme learning machines; Linear least-squares; Random feature methods; Multiscale PDEs.

1 Introduction

Accurate and efficient numerical solution of partial differential equations (PDEs) remains a central challenge in computational science and engineering. Classical discretisation techniques such as finite difference and finite element methods have matured into highly reliable tools, yet they can become costly or difficult to apply in problems involving high dimensionality, complex geometries, or strongly multiscale behaviour. These challenges have motivated increasing interest in alternative computational paradigms capable of combining flexible function approximation with physical constraints. In recent years, *scientific machine learning* (SciML) has emerged as a promising framework for tackling such problems. Among the various approaches proposed in this area, *physics-informed neural networks* (PINNs) [1, 2] have attracted considerable attention. In PINNs, the solution of a PDE is approximated by a neural network whose parameters are trained by minimising a loss function that penalises the residual of the governing PDE and its boundary conditions. This formulation allows PDE solving to be recast as a continuous optimisation problem and offers several appealing features, including mesh-free discretisation, straightforward implementation through automatic differentiation, and a unified framework for forward and inverse problems.

Despite these advantages, standard PINNs trained via gradient-based optimisation exhibit several well-documented difficulties. Training can be slow and sensitive to hyperparameters, and the resulting optimisation problem is often poorly conditioned. Moreover, neural networks trained by gradient descent are known to display a *spectral bias* toward low-frequency functions [3], which limits their ability to resolve highly oscillatory or multiscale solutions. As a result, classical PINNs frequently struggle with problems containing high-frequency content or widely separated spatial scales [4]. To address these limitations, a variety of domain decomposition strategies have been proposed. Conservative PINNs (cPINNs) [5] enforce flux continuity across non-overlapping subdomains, while extended PINNs (XPINNs) [6] allow flexible space–time decompositions.

A particularly effective approach is the *Finite Basis Physics-Informed Neural Network* (FBPINN) method introduced by Moseley et al. [4]. In FBPINNs, the computational domain is decomposed into overlapping subdomains, each equipped with a small neural network whose output is multiplied by a smooth window function forming a partition of unity. The global solution is obtained by summing the local contributions across all subdomains. This localisation substantially mitigates spectral bias by reducing the complexity of the function each network must approximate [7, 8]. Nevertheless, FBPINNs still rely on gradient-based training of all network parameters, which remains computationally expensive and can limit robustness.

An alternative strategy is to replace fully trainable neural networks with *random feature models*. In particular, *Extreme Learning Machines* (ELMs) [9] fix the hidden-layer weights at random and determine only the output weights by solving a linear least-squares problem. This idea transforms training from a nonlinear optimisation problem into a linear algebra problem and is closely related to the *Random Feature Method* (RFM) [10]. Randomised neural network models have a long history, including random vector functional-link networks [11] and reservoir computing [12], and have recently been applied to PDE solving. Examples include the Local Extreme Learning Machine method of Dong and Li [13], distributed learning machine approaches [14], and the Extreme Theory of Functional Connections framework [15]. These methods demonstrate that fixed random features can provide competitive accuracy while dramatically simplifying training [10, 16, 17].

In this work, we investigate the combination of these two ideas: domain localisation and random feature approximation. Specifically, we replace the trainable subdomain networks in the FBPINN framework with extreme learning machines, yielding a method we refer to as *ELM-FBPINN*. A preliminary study was performed in the first version of [16]. In the current work, we go one step further by pushing deeper the study of its performance and exploring numerically both a one-level method and its multi-level generalisation. The resulting formulation retains the partition-of-unity domain decomposition structure of FBPINNs while eliminating gradient-based optimisation entirely. Instead, the PDE solution is obtained by solving a global linear least-squares system for the output weights associated with randomly initialised basis functions.

This reformulation raises several fundamental questions regarding the role of optimisation, localisation, and model capacity in physics-informed learning. In particular, we seek to understand whether replacing nonlinear optimisation with linear least-squares solves can improve robustness and convergence behaviour without sacrificing accuracy, and how the resulting method behaves as problem difficulty and model capacity vary. The present study is therefore guided by the following research questions:

- **RQ1:** Does replacing gradient-based optimisation with a linear least-squares formulation improve convergence speed and robustness while maintaining solution accuracy?
- **RQ2:** To what extent does domain localisation mitigate spectral bias and enable accurate approximation of highly oscillatory or multiscale solutions?
- **RQ3:** How does the number of random basis functions per subdomain influence model expressivity, redundancy, and the conditioning of the resulting least-squares system?
- **RQ4:** Can the method maintain stable performance as problem difficulty increases when model capacity is scaled accordingly, and can multilevel modeling improve this performance?

To address these questions, we compare three architectures: a standard PINN, an FBPINN, and the proposed ELM-FBPINN. This comparison allows us to isolate the effects of domain decomposition and training strategy independently. The methods are evaluated on two benchmark problems: a one-dimensional damped harmonic oscillator,

which exhibits highly oscillatory temporal dynamics, and a two-dimensional multiscale Laplace problem designed to test spatial multiscale behaviour.

Through these experiments, we aim to clarify the respective roles of localisation, random feature representations, and linear least-squares formulations in physics-informed neural networks. More broadly, the results contribute to an emerging perspective in which neural PDE solvers are viewed not only as trainable black-box models but also as approximation schemes whose design choices directly influence their numerical behaviour.

2 Related work

The present work can be viewed as a generalisation of the random feature formulation introduced in the first version of [16], extending it to a multilevel domain-decomposition setting. It is also closely related to the Random Feature Method (RFM) proposed in [10]. The main differences with respect to [10] lie in the treatment of domain localisation and the exploitation of sparsity. In the present work, the neural basis functions are organised through a domain-decomposition framework and evaluated only on the collocation points associated with their corresponding subdomains. This leads to a naturally sparse system matrix, which we explicitly exploit by assembling the matrix in sparse form and solving the resulting least-squares problem using sparse iterative solvers. In contrast, existing RFM formulations typically construct dense systems and do not exploit the sparsity induced by localisation.

Several recent works have also explored random-feature and frozen-network approaches for PDE solvers, including multiscale and domain-decomposition settings. In particular, [18] proposes a multiscale PDE solver based on domain decomposition and random features, and [19] introduces frozen physics-informed neural networks to accelerate training through linear least-squares formulations. Finally, other works have investigated preconditioning strategies for random-feature-based PDE solvers. In particular, [20] and [21] propose preconditioning techniques aimed at improving the conditioning of the resulting least-squares systems and do not consider multilevel formulations.

While these works share the same general philosophy of replacing gradient-based training with linear solvers, the present study provides a more thorough assessment of the multilevel domain-decomposition framework, with a particular focus on approximation properties, sparsity structure, conditioning, and scalability. In particular, we explicitly study how localisation, multilevel decomposition, and basis enrichment interact, and how these design choices affect accuracy, robustness, and computational efficiency.

3 The multilevel ELM-FBPINN method

We now extend the random-feature FBPINN formulation introduced in [16] and used in [21] to a multilevel domain-decomposition setting. The goal is to retain the localization advantages of the FBPINN framework while replacing gradient-based training by a linear least-squares solve using randomised neural features.

We start with a PDE defined in a domain $\Omega \subset \mathbb{R}^d$

$$\mathcal{N}[u(\mathbf{x})] = f(\mathbf{x}), \quad \mathbf{x} \in \Omega,$$

under boundary conditions given by

$$\mathcal{B}_b[u(\mathbf{x})] = g_b(\mathbf{x}), \quad \mathbf{x} \in \Gamma_b \subset \partial\Omega, \quad b = 1, \dots, B,$$

where \mathcal{N} and the \mathcal{B}_b are assumed to be linear operators and f and g_b are forcing and boundary functions. Instead of using a single decomposition into J subdomains, we introduce a hierarchy of decompositions indexed by levels $\ell = 1, \dots, L$. At each level ℓ , the domain is covered by J_ℓ overlapping subdomains $\Omega = \bigcup_{j=1}^{J_\ell} \Omega_j^{(\ell)}$. Associated with these subdomains are compactly supported window functions $\{\omega_j^{(\ell)}(\mathbf{x})\}_{j=1}^{J_\ell}$, which form a partition of unity at each level,

$$\sum_{j=1}^{J_\ell} \omega_j^{(\ell)}(\mathbf{x}) = 1, \quad \mathbf{x} \in \Omega.$$

Typically the decompositions become progressively finer as the level increases, so that level $\ell = 1$ corresponds to a coarse representation of the solution and higher levels introduce increasingly localised corrections. Using this hierarchy, we approximate the PDE solution as a sum of localised random feature expansions across all levels,

$$\hat{u}(\mathbf{x}, \mathbf{a}) = \frac{1}{L} \sum_{\ell=1}^L \sum_{j=1}^{J_\ell} \omega_j^{(\ell)}(\mathbf{x}) \sum_{k=1}^K a_{jk}^{(\ell)} \phi_{jk}^{(\ell)}(\mathbf{x}, \theta_{jk}^{(\ell)}). \quad (1)$$

Here $\phi_{jk}^{(\ell)}(\mathbf{x}, \theta_{jk}^{(\ell)})$ are neural network basis functions, K denotes the number of random features per subdomain and $a_{jk}^{(\ell)}$ are trainable output weights. As in the single-level formulation, the neural features are taken to be shallow fully connected networks

$$\begin{aligned} \mathbf{z}_j^{(\ell,0)} &= \mathbf{x}, \\ \mathbf{z}_j^{(\ell,m)} &= \Xi \left(W_j^{(\ell,m)} \mathbf{z}_j^{(\ell,m-1)} + \mathbf{b}_j^{(\ell,m)} \right), \quad m = 1, \dots, h-1, \\ \phi_{jk}^{(\ell)}(\mathbf{x}, \theta_{jk}^{(\ell)}) &= \Xi \left((\mathbf{w}_{jk}^{(\ell)})^\top \mathbf{z}_j^{(\ell,h-1)} \right), \end{aligned} \quad (2)$$

where Ξ is a nonlinear activation function applied elementwise. The parameters

$$\theta_{jk}^{(\ell)} = \{W_j^{(\ell,m)}, \mathbf{b}_j^{(\ell,m)}\}_{m=1}^{h-1} \cup \{\mathbf{w}_{jk}^{(\ell)}\}$$

are randomly initialised and then kept fixed. Consequently, only the coefficients $a_{jk}^{(\ell)}$ remain as unknown parameters. This formulation therefore produces a multilevel

random-feature approximation in which each level contributes localised neural basis functions with support determined by the window functions $\omega_j^{(\ell)}$.

The unknown coefficients are determined by minimizing the physics-informed loss functional

$$\mathcal{L}(\mathbf{a}) = \frac{1}{N_I} \sum_{n=1}^{N_I} (\mathcal{N}[\hat{u}(\mathbf{x}_n, \mathbf{a})] - f(\mathbf{x}_n))^2 + \sum_{b=1}^B \frac{\lambda_b}{N_B^{(b)}} \sum_{i=1}^{N_B^{(b)}} \left(\mathcal{B}_b[\hat{u}(\mathbf{x}_i^{(b)}, \mathbf{a})] - g_b(\mathbf{x}_i^{(b)}) \right)^2. \quad (3)$$

Here $\{\mathbf{x}_n\}_{n=1}^{N_I}$ are interior collocation points and $\{\mathbf{x}_i^{(b)}\}_{i=1}^{N_B^{(b)}}$ are boundary collocation points associated with boundary operators \mathcal{B}_b . Since the operators \mathcal{N} and \mathcal{B}_b are linear, the loss functional remains quadratic in the coefficients \mathbf{a} even in the multilevel setting. Consequently, the training problem reduces to a linear least-squares problem.

Let $N_\Phi = \sum_{\ell=1}^L J_\ell K$ denote the total number of random features across all levels. The parameter vector collects all coefficients $\mathbf{a} = \{a_{jk}^{(\ell)}\} \in \mathbb{R}^{N_\Phi}$. Proceeding as in [21], the loss functional can be written as

$$\min_{\mathbf{a} \in \mathbb{R}^{N_\Phi}} \|\mathbf{N}\mathbf{a} - \mathbf{f}\|^2 + \|\mathbf{B}\mathbf{a} - \mathbf{g}\|^2, \quad (4)$$

where \mathbf{N} and \mathbf{B} denote the system matrices associated with the PDE residuals and the boundary conditions, respectively. The vectors \mathbf{f} and \mathbf{g} contain evaluations of the forcing term and boundary terms at interior and boundary collocation points, respectively.

As in the single-level formulation, the two residual contributions can be combined into a single global least-squares problem

$$\min_{\mathbf{a} \in \mathbb{R}^{N_\Phi}} \|\mathbf{M}\mathbf{a} - \mathbf{h}\|^2, \quad \text{where } \mathbf{M} = \begin{bmatrix} \mathbf{N} \\ \mathbf{B} \end{bmatrix}, \quad \mathbf{h} = \begin{bmatrix} \mathbf{f} \\ \mathbf{g} \end{bmatrix}. \quad (5)$$

Indexing conventions

To describe the structure of the system matrices, we introduce the following indexing conventions.

- Let $q = \sum_{m=1}^{\ell-1} J_m K + (j-1)K + k$ map the triple (ℓ, j, k) to a global column index.
- Let $p = \sum_{m=1}^{b-1} N_B^{(m)} + i$ map the pair (i, b) to a global boundary collocation index.

We also denote $N_B = \sum_{b=1}^B N_B^{(b)}$ as the total number of boundary collocation points.

Definition of vectors

The vectors appearing in (5) are defined as

$$\mathbf{f} = \left\{ \frac{1}{\sqrt{N_I}} f(\mathbf{x}_n) \right\}_{n=1}^{N_I}, \quad \mathbf{g} = \{g_p\}_{p=1}^{N_B}, \quad g_p = \sqrt{\frac{\lambda_b}{N_B^{(b)}}} g_b(\mathbf{x}_i^{(b)}).$$

Definition of the system matrices

The matrices $\mathbf{N} \in \mathbb{R}^{N_I \times N_\Phi}$ and $\mathbf{B} \in \mathbb{R}^{N_B \times N_\Phi}$ are defined componentwise by

$$N_{n,q} = \frac{1}{\sqrt{N_I}L} \mathcal{N} \left[(\omega_j^{(\ell)} \phi_{jk}^{(\ell)})(\mathbf{x}_n) \right], \quad B_{p,q} = \sqrt{\frac{\lambda_b}{N_B^{(b)}}} \frac{1}{L} \mathcal{B}_b \left[(\omega_j^{(\ell)} \phi_{jk}^{(\ell)})(\mathbf{x}_i^{(b)}) \right].$$

Each column therefore corresponds to the action of the PDE or boundary operator applied to a localised random feature $\omega_j^{(\ell)}(\mathbf{x})\phi_{jk}^{(\ell)}(\mathbf{x})$.

Multilevel domain-decomposition structure

Because the window functions $\omega_j^{(\ell)}$ have compact support, the resulting matrix

$$\mathbf{M} \in \mathbb{R}^{(N_I+N_B) \times N_\Phi}$$

is sparse. In particular, an entry $M_{r,q}$ is nonzero only when $\omega_j^{(\ell)}(\mathbf{x}_r) \neq 0$. We therefore define the index sets

$$I_j^{(\ell)} = \{r \mid \omega_j^{(\ell)}(\mathbf{x}_r) \neq 0\}, \quad K_j^{(\ell)} = \left\{ \sum_{m=1}^{\ell-1} J_m K + (j-1)K + 1, \dots, \sum_{m=1}^{\ell-1} J_m K + jK \right\},$$

where $I_j^{(\ell)}$ contains the rows corresponding to collocation points influenced by subdomain j at level ℓ , and $K_j^{(\ell)}$ contains the associated feature indices. Let

$$\mathbf{M}_j^{(\ell)} = \mathbf{M}|_{I_j^{(\ell)} \times K_j^{(\ell)}}$$

denote the corresponding submatrix. Introducing restriction matrices

$$\mathbf{V}_j^{(\ell)} \in \mathbb{R}^{|I_j^{(\ell)}| \times (N_I+N_B)}, \quad \mathbf{W}_j^{(\ell)} \in \mathbb{R}^{K \times N_\Phi},$$

we can write

$$\mathbf{M}_j^{(\ell)} = \mathbf{V}_j^{(\ell)} \mathbf{M} \mathbf{W}_j^{(\ell)T}.$$

This yields the multilevel decomposition

$$\mathbf{M} = \sum_{\ell=1}^L \sum_{j=1}^{J_\ell} \mathbf{V}_j^{(\ell)T} \mathbf{M}_j^{(\ell)} \mathbf{W}_j^{(\ell)}. \quad (6)$$

Equation (6) reveals the hierarchical block-sparse structure of the system matrix induced by the multilevel domain decomposition. An example plot of this sparse structure is shown in Figure 1. In practice, this structure enables efficient assembly of \mathbf{M} using sparse data structures and efficient solution of (5) using iterative least-squares solvers such as LSQR. Once the coefficient vector \mathbf{a} has been computed, the approximate solution \hat{u} can be evaluated at arbitrary points by assembling the corresponding localised random feature expansions across all levels.

	PINN	FBPINN	ELM-FBPINN
Domain decomposition / POU	✗	✓	✓
Local (subdomain) models	✗	✓	✓
Hidden features trainable?	✓	✓	✗
Training strategy	GD (Adam)	GD (Adam)	LS solver (e.g. LSQR)
Unknowns solved for	all weights	all weights	output weights only
Linear solve required?	✗	✗	✓
Expected effect	spectral bias	mitigates bias	mitigates bias + faster solve

Table 1: Summary of the three compared approaches.

4 Numerical assessment of the ELM-FBPINN method

Our objective is to assess whether replacing gradient-based subdomain training by a random-feature least-squares solve can improve the efficiency and robustness of physics-informed solvers without sacrificing accuracy. To isolate the effect of the training strategy from the effect of domain localisation, we compare three models: (i) a standard single-domain PINN trained by gradient descent, (ii) an FBPINN that uses a domain decomposition and partition-of-unity construction and trainable subdomain networks, and (iii) the proposed ELM-FBPINN, which retains the FBPINN domain decomposition and partition-of-unity structure while replacing each subdomain network by a random-feature model and solving for the output coefficients via least squares (Table 1). We also assess the performance impact of including multiple levels in the ELM-FBPINN. Two representative test cases are considered:

- **1D damped harmonic oscillator.** This problem yields oscillatory solutions with controlled frequency content and exponential decay. It provides a controlled setting to probe spectral bias, the benefit of domain localisation, and the scaling of solver performance as the oscillation frequency increases.
- **2D multi-scale Laplace problem.** This elliptic PDE admits an analytic solution composed of multiple sine modes, allowing systematic control of multiscale complexity in a higher-dimensional setting.

The numerical study is designed to isolate the influence of a small number of experimental parameters corresponding to the research questions introduced in Section 1. In particular, we vary the following levers:

- **RQ1: Training strategy**-gradient descent (GD) versus linear least-squares (LSQ).
- **RQ2: Domain localisation**-number of subdomains J_l .
- **RQ3: Basis enrichment**-number of basis functions per subdomain K .
- **RQ4: Problem difficulty**-frequency or multiscale content scaled with J_l , and assessing the impact of including multiple levels, L .

Although it is also possible to alter the depth (h) of the networks used, preliminary experiments indicated that this did not offer much benefit, and that shallow networks

were optimal or near-optimal. The comparisons in Table 1 and the research questions define our experimental framework. By separating localisation (shared by FBPINN and ELM-FBPINN) from training strategy (gradient descent versus least-squares), and by systematically varying capacity, and problem difficulty, the numerical study is designed to disentangle approximation effects from optimisation effects.

4.1 Common implementation details

We now describe the common implementation choices used across all experiments which also represent a practical compromise as there are many possible choices of hyperparameters. These details ensure that comparisons are fair and that observed differences can be attributed to structural properties of the methods rather than to incidental training or sampling choices. Several aspects of the training and evaluation setup are shared across all experiments in one and two dimensions. Unless stated otherwise, the settings introduced below are fixed throughout all numerical experiments.

Domain decomposition

Both the FBPINN and ELM-FBPINN employ the same domain decomposition strategy. We assume that the global computational domain has a tensor-product structure,

$$\Omega = \bigotimes_{i=1}^d [x_{\min}^i, x_{\max}^i],$$

and at each level, ℓ , we decompose Ω into overlapping equally sized intervals in one dimension and overlapping rectangular subdomains arranged on a uniform grid in two dimensions. Example domain decompositions in one and two dimensions are shown in Figures 1 and 7.

Localisation is enforced through a partition-of-unity (POU) construction at each level. The window functions are defined as

$$\omega_j^{(\ell)}(\mathbf{x}) = \frac{\hat{\omega}_j^{(\ell)}(\mathbf{x})}{\sum_{j=1}^{J_\ell} \hat{\omega}_j^{(\ell)}(\mathbf{x})}, \quad \hat{\omega}_j^{(\ell)}(\mathbf{x}) = \prod_{i=1}^d \left[1 + \cos\left(\pi \frac{x_i - \mu_{ji}^{(\ell)}}{\sigma_{ji}^{(\ell)}}\right) \right]^2, \quad (7)$$

where $\mu_{ji}^{(\ell)}$ and $\sigma_{ji}^{(\ell)}$ denote the centre and half-width of the j th subdomain in dimension i at level ℓ . For a one-dimensional domain, the subdomain bounds are defined as

$$x_{j,\min}^{(\ell)} = \mu_j^{(\ell)} - \frac{\delta}{2}(\mu_j^{(\ell)} - \mu_{j-1}^{(\ell)}), \quad x_{j,\max}^{(\ell)} = \mu_j^{(\ell)} + \frac{\delta}{2}(\mu_{j+1}^{(\ell)} - \mu_j^{(\ell)}), \quad (8)$$

with $\mu_j^{(\ell)}$ equally spaced over the domain and $\sigma_{ji}^{(\ell)} = (x_{j,\max}^{(\ell)} - x_{j,\min}^{(\ell)})/2$, where δ is a width ratio that controls the degree of overlap and therefore information exchange between subdomains. An analogous definition is used for two dimensional domains with the same δ along each dimension. Note that a width ratio of less than one means that the subdomains no longer overlap. This cosine-based construction yields smooth

window functions with compact support, ensuring locality while preserving a smooth global approximation.

Neural network architecture and weight initialisation

All models employ fully connected neural networks with tanh activation functions. In the PINN and FBPINN models, all network parameters are trainable. In contrast, the ELM-FBPINN fixes the hidden-layer parameters after random initialisation and trains only the linear output coefficients. All network weights are initialised using uniform LeCun initialisation [22], i.e. randomly sampled according to $W_j^{(\ell,m)}, b_j^{(\ell,m)} \sim \mathcal{U}(-a, a)$, where $a = R\sqrt{\frac{1}{\dim(\mathbf{z}^{(\ell,m-1)})}}$. Here R is a positive parameter which we use to test the sensitivity of our models to the magnitude of the initialized weights.

Optimisation and solvers

The PINN and FBPINN models are trained using the Adam optimiser with a learning rate of 10^{-3} for 15,000 iterations. The ELM-FBPINN replaces gradient-based optimisation with a sparse linear least-squares solve, which is performed using the iterative LSQR solver from SciPy [23], with a maximum of 15,000 iterations. Unless stated otherwise, the solver is allowed to run for the full iteration budget in order to facilitate direct comparison of convergence behaviour. In practice, many problems studied here converge much faster than the maximum number iterations and could be stopped early with an appropriate stopping condition. Model performance is assessed using the normalised L^1 test accuracy given by

$$e_{L^1} = \frac{1}{M\varsigma} \sum_{i=1}^M |\hat{u}(\mathbf{x}_i) - u(\mathbf{x}_i)|, \quad (9)$$

where M is the number of test points, and ς is the standard deviation of the set of true solutions $\{u(\mathbf{x}_i)\}_i^M$. Training and test points are sampled on a regular grid, with sufficient resolution per subdomain to accurately capture local approximation quality. For fairness exactly the same collocation points and random seeds are used for each model compared (PINN/FBPINN/ELM-FBPINN). For robustness each model is retrained using five independent random seeds, and test accuracies are reported as the median value, with error bars indicating the range between the best and worst observed values. Training times are reported as the mean with error bars indicating one standard deviation. For the ELM-FBPINN, training time includes every stage of the computation; construction of the local bases, assembly of the global system, and iterative solution time.

Software and hardware implementation

All models are implemented in Python using JAX [24], building upon the highly optimised open-source FBPINN library [4]. All models are trained on a single AMD EPYC 7742 CPU core with 50 GB RAM, using the SciPy library [25] for defining sparse linear solvers.

4.2 1D problem – Damped harmonic oscillator

The damped harmonic oscillator provides a controlled setting in which the solution exhibits oscillations with tunable frequency and exponential decay. This setting probes robustness to increasing frequency, the benefit of domain decomposition, and the effect of replacing nonlinear optimisation by a linear least-squares solve.

Problem definition

We consider the displacement $u(t)$ on $t \in (0, 1]$ governed by

$$\begin{cases} mu_{tt} + \mu u_t + ku(t) = 0, & t \in (0, 1], \\ u(0) = u_0, \quad u_t(0) = v_0, \end{cases} \quad (10)$$

where m is the mass, μ the damping coefficient, and k the spring constant.

Under-damped regime and tunable frequency

Defining

$$\beta = \frac{\mu}{2m}, \quad \omega_0 = \sqrt{\frac{k}{m}},$$

the under-damped regime corresponds to $\beta < \omega_0$, with oscillation frequency

$$\omega = \sqrt{\omega_0^2 - \beta^2}.$$

We fix $u_0 = 1$, $v_0 = 0$, $m = 1$ and $\mu = 4$ (hence $\beta = 2$) and vary ω_0 to control difficulty: increasing ω_0 introduces higher-frequency components while preserving the decay rate. The exact solution is

$$u(t) = e^{-\beta t} 2A \cos(\phi + \omega t), \quad (11)$$

with

$$A = \frac{u_0}{2 \cos(\phi)}, \quad \phi = \arctan\left(-\frac{(v_0/u_0) + \beta}{\omega}\right).$$

Physics-informed objective

All models minimise the same residual-based loss,

$$\mathcal{L} = \mathcal{L}_{\text{phys}} + \lambda_{u_0} \mathcal{L}_{\text{ic}}^{(u_0)} + \lambda_{v_0} \mathcal{L}_{\text{ic}}^{(v_0)}, \quad (12)$$

with

$$\mathcal{L}_{\text{phys}} = \frac{1}{N_I} \sum_{i=1}^{N_I} (m\hat{u}_{tt} + \mu\hat{u}_t + k\hat{u})^2(t_i), \quad (13)$$

$$\mathcal{L}_{\text{ic}}^{(u_0)} = (\hat{u}(0) - u_0)^2, \quad (14)$$

$$\mathcal{L}_{\text{ic}}^{(v_0)} = (\hat{u}_t(0) - v_0)^2. \quad (15)$$

We fix $\lambda_{u_0} = 10^6$ and $\lambda_{v_0} = 10^2$ to enforce the initial conditions, finding this gives a reasonable balance between all loss terms.

Summary of observed behaviour

On highly oscillatory instances, a standard PINN fails to converge within the training budget, whereas both FBPINN and ELM-FBPINN converge reliably. Across ablations, ELM-FBPINN attains comparable or lower errors than FBPINN while converging faster, provided each subdomain has sufficient local capacity. Failure modes are dominated by insufficient localisation (small J_l) or feature degeneracy (small K), rather than optimisation speed alone.

Ablation roadmap

Starting from a baseline configuration, we vary (i) local capacity (K), (ii) localisation resolution (J_l), and (iii) frequency scaling via coupled ω_0 and J_l , comparing one-level with multilevel models. When relevant, we report the condition number and numerical rank of the ELM-FBPINN system matrix to interpret stability trends.

4.2.1 Baseline

We consider the under-damped oscillator with $\omega_0 = 80$, yielding a highly oscillatory solution with slowly decaying amplitude. The PINN uses $h = 2$ hidden layers and $K = 64$ basis functions per layer. Both the FBPINN and ELM-FBPINN use a single hidden layer ($h = 1$) with $K = 12$ basis functions per subdomain, and a one-level decomposition into $J_1 = 20$ subdomains with width ratio $\delta = 2.9$. All models use a weight scaling of $R = 1$ and are trained on 260 regularly spaced collocation points.

Figure 2 shows the test error with $M = 1000$ regularly spaced test points versus iteration count. The PINN does not converge to an acceptable solution within the training budget, consistent with the well-known difficulty of gradient-based PINNs in resolving high-frequency components. Both decomposed methods converge, and ELM-FBPINN reaches the lowest final error while converging faster than FBPINN. While PINN fails to capture the real solution leading to large errors, the two decomposed methods yield similar predictions. Table 2 summarises final test errors and wall-clock times. In this baseline, ELM-FBPINN attains the best median accuracy with a faster training time to the PINN and FBPINN.

Network	(ω_0, J)	(h, K)	δ	$\kappa(M)$	Optimiser	e_{L_1}	Time (s)
FCN	(80, 1)	(2, 64)	2.9	N/A	PINN-Adam	$5.5 \pm 0.4e-01$	$3.3 \pm 0.1e+01$
FCN	(80, 20)	(1, 12)	2.9	N/A	FBPINN-Adam	$1.1 \pm 0.4e-03$	$2.5 \pm 0.1e+01$
ELM	(80, 20)	(1, 12)	2.9	$2.2e+18$	LSQR	$1.1 \pm 0.6e-04$	5.1 ± 0.1

Table 2: Baseline results for the 1D damped harmonic oscillator, where J lists the number of subdomains for each level (here, in all cases $L = 1$).

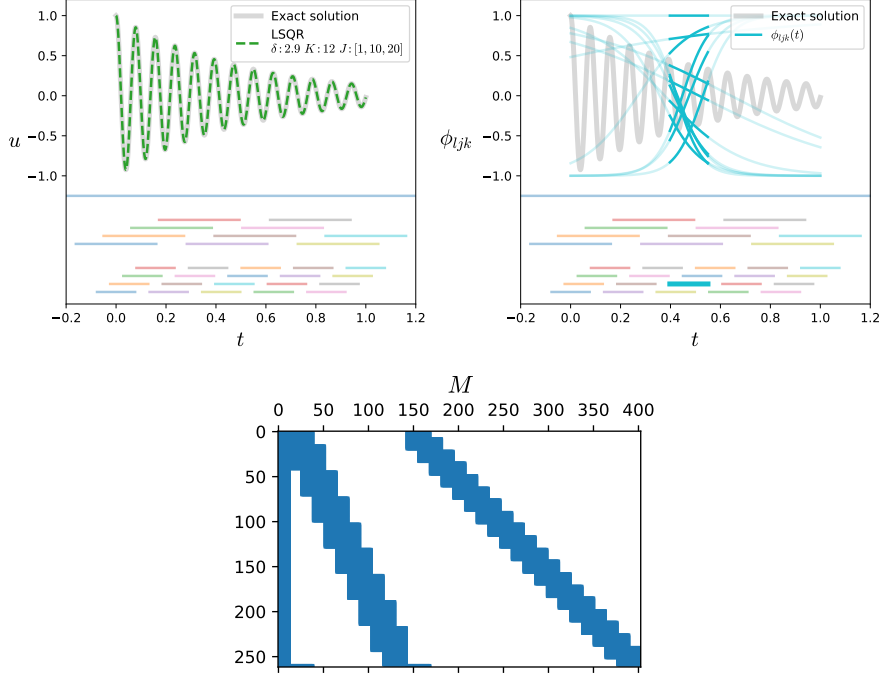


Fig. 1: Model predictions versus the exact solution for the 1D damped harmonic oscillator with a multilevel ELM-FBPINN, where J lists the number of subdomains for each level; basis functions generated by randomisation; sparse multilevel structure of M .

We also show the model predictions in Figure 1 for the same ELM-FBPINN, but with $L = 3$ and $J = [1, 10, 20]$ subdomains, where J lists the number of subdomains for each level (i.e., $J_1 = 1$, $J_2 = 10$, and $J_3 = 20$). The multilevel solution is visually indistinguishable from the exact solution. The figure also illustrates the randomly generated basis functions and the sparse multilevel structure of the system matrix M , which is a key feature of the proposed approach.

4.2.2 Varying number of basis functions

We vary the number of basis functions K of the baseline $L = 1$ model to probe how each method exploits increased local capacity. This ablation distinguishes (i) expressivity limitations at small K from (ii) redundancy/feature correlation at large K . Convergence curves and final errors are shown in Figure 3 and Table 3.

Key observations

(i) All PINN configurations fail to converge, even as K increases, reinforcing that additional capacity alone does not resolve the optimisation difficulty on this high-frequency

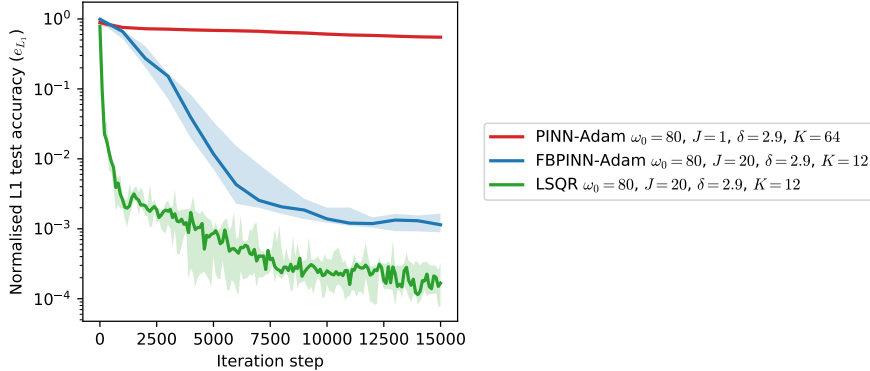


Fig. 2: Logarithm of the L^1 test error versus iteration count for the baseline 1D damped harmonic oscillator, where J lists the number of subdomains for each level (here, in all cases $L = 1$).

problem. (ii) Both decomposed methods converge for moderate K , but ELM-FBPINN is the only method that shows a strong and systematic improvement with increasing K before saturating. (iii) At very small K , FBPINN can outperform ELM-FBPINN: in this low-capacity regime, the random-feature trial space is too limited to generalise accurately, and the linear solve cannot compensate for missing expressivity.

For the ELM-FBPINN, the error decreases rapidly as the number of basis functions K increases from very small values, and then plateaus for larger K , indicating that once the dominant oscillatory structure is resolved, additional basis functions provide diminishing returns. This occurs despite a rapid increase in the condition number $\kappa(M)$, suggesting growing linear dependence among the random basis functions, although the least-squares solver remains stable in practice. In contrast, the PINN shows only marginal improvement as K increases while the computational cost grows significantly, whereas the FBPINN reaches good accuracy for moderate K but also plateaus. Overall, the ELM-FBPINN achieves the lowest errors across all tested values of K while maintaining faster runtimes, since training reduces to the solution of a linear least-squares problem rather than iterative gradient-based optimisation.

Interpretation via linear-system diagnostics

As K increases, $\kappa(\mathbf{M})$ grows rapidly and the numerical rank saturates, consistent with the introduction of increasingly correlated random features. This provides a qualitative explanation for the observed accuracy plateau: beyond moderate K , additional basis functions add limited independent information.

Overall, except for very small K ($K = 2, 4$), ELM-FBPINN outperforms both FBPINN and PINN in accuracy while avoiding gradient-based optimisation. Despite the growth of $\kappa(\mathbf{M})$ with K , the least-squares problems are evidently solved well enough to obtain accurate ELM-FBPINN solutions. This suggests that the full least-squares system is not as numerically problematic as $\kappa(\mathbf{M})$ alone might indicate.

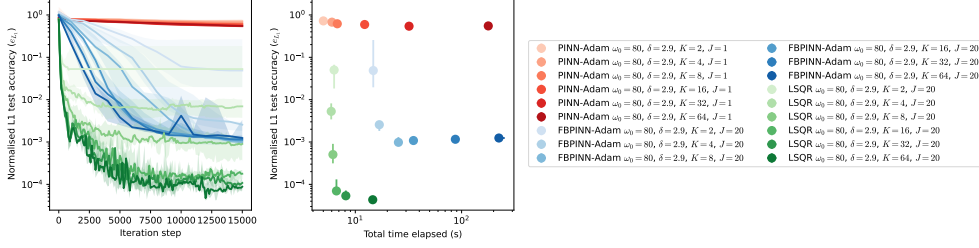


Fig. 3: All models e_{L^1} vs number of basis functions, K , for the 1D damped harmonic oscillator, where J lists the number of subdomains, for each level (here, in all cases $L = 1$).

Network	(ω_0, J)	(h, K)	δ	$\kappa(M)$	Optimiser	e_{L^1}	Time (s)
FCN	(80, 1)	(2, 2)	2.9	N/A	PINN-Adam	$7.2 \pm 0.2e-01$	5.0 ± 0.2
FCN	(80, 1)	(2, 4)	2.9	N/A	PINN-Adam	$6.8 \pm 0.2e-01$	6.0 ± 0.1
FCN	(80, 1)	(2, 8)	2.9	N/A	PINN-Adam	$6.2 \pm 1.0e-01$	6.8 ± 0.2
FCN	(80, 1)	(2, 16)	2.9	N/A	PINN-Adam	$6.0 \pm 1.1e-01$	$1.2 \pm 0.0e+01$
FCN	(80, 1)	(2, 32)	2.9	N/A	PINN-Adam	$5.4 \pm 0.3e-01$	$3.2 \pm 0.1e+01$
FCN	(80, 1)	(2, 64)	2.9	N/A	PINN-Adam	$5.5 \pm 0.4e-01$	$1.8 \pm 0.0e+02$
FCN	(80, 20)	(1, 2)	2.9	N/A	FBPINN-Adam	$4.9 \pm 23.7e-02$	$1.5 \pm 0.0e+01$
FCN	(80, 20)	(1, 4)	2.9	N/A	FBPINN-Adam	$2.6 \pm 1.1e-03$	$1.7 \pm 0.0e+01$
FCN	(80, 20)	(1, 8)	2.9	N/A	FBPINN-Adam	$9.8 \pm 4.7e-04$	$2.5 \pm 0.0e+01$
FCN	(80, 20)	(1, 16)	2.9	N/A	FBPINN-Adam	$1.1 \pm 0.3e-03$	$3.5 \pm 0.1e+01$
FCN	(80, 20)	(1, 32)	2.9	N/A	FBPINN-Adam	$1.2 \pm 0.1e-03$	$8.7 \pm 0.5e+01$
FCN	(80, 20)	(1, 64)	2.9	N/A	FBPINN-Adam	$1.2 \pm 0.1e-03$	$2.2 \pm 0.2e+02$
ELM	(80, 20)	(1, 2)	2.9	$2.7e+05$	LSQR	$5.0 \pm 4.8e-02$	6.3 ± 0.0
ELM	(80, 20)	(1, 4)	2.9	$6.0e+08$	LSQR	$5.3 \pm 4.7e-03$	5.9 ± 0.1
ELM	(80, 20)	(1, 8)	2.9	$3.7e+16$	LSQR	$5.1 \pm 5.9e-04$	6.2 ± 0.1
ELM	(80, 20)	(1, 16)	2.9	$9.5e+18$	LSQR	$7.0 \pm 6.6e-05$	6.6 ± 0.2
ELM	(80, 20)	(1, 32)	2.9	$2.4e+19$	LSQR	$5.4 \pm 2.6e-05$	8.1 ± 0.2
ELM	(80, 20)	(1, 64)	2.9	$1.5e+20$	LSQR	$4.3 \pm 1.1e-05$	$1.5 \pm 0.0e+01$

Table 3: Final e_{L^1} values and total run time for each model at different number of basis functions, K , for the 1D damped harmonic oscillator, where J lists the number of subdomains for each level (here, in all cases $L = 1$).

4.2.3 Varying number of subdomains

We vary the number of subdomains J_1 of the baseline $L = 1$ model to test how localisation affects approximation quality and convergence. Unlike increasing K , increasing J_1 primarily adds *spatially distinct* basis functions, which should improve representation of highly oscillatory solutions once subdomains are sufficiently small.

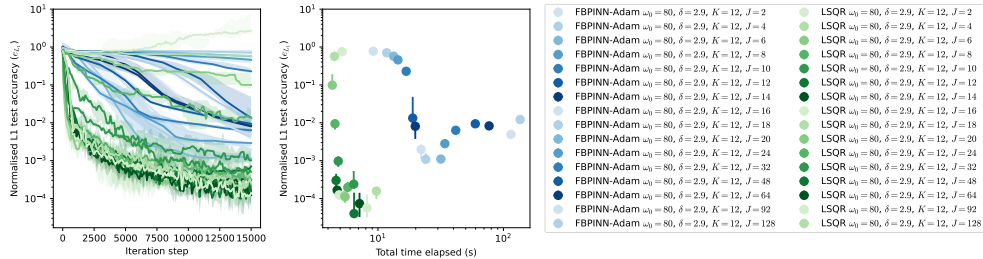


Fig. 4: All models e_{L^1} vs number of subdomains, J , for FBPINN and ELM-FBPINN, for the 1D damped harmonic oscillator, where J lists the number of subdomains for each level (here, in all cases $L = 1$).

Key observations

Figure 4 shows that both methods improve with increasing J_1 , but a minimum level of localisation is required: $J_1 = 2$ and $J_1 = 4$ fail to converge reliably for either approach. For $J_1 \gtrsim 8$, ELM-FBPINN converges faster than FBPINN and typically attains lower errors. Final errors and times are summarised in Table 4. Accuracy improves significantly as the number of subdomains J_1 increases from very small values, reflecting the benefit of domain localisation for resolving the oscillatory structure of the solution. The error decreases rapidly up to moderate values of J_1 (approximately $J_1 = 12$ – 20), after which accuracy saturates and may slightly degrade for very large J_1 , indicating diminishing returns once each local subproblem becomes sufficiently simple and the decomposition becomes excessively fine. In contrast to increasing K , increasing J_1 does not dramatically worsen $\kappa(\mathbf{M})$, which remains in the range 10^{17} – 10^{19} , while the numerical rank grows approximately linearly with J_1 , indicating that additional subdomains introduce largely independent degrees of freedom. This supports the interpretation that increasing J_1 expands the trial space by adding spatially distinct basis functions rather than correlated features. Finally, we observe that the computational cost grows significantly with J_1 for FBPINN due to the increased optimisation cost, whereas for ELM-FBPINN the runtime increases only mildly.

4.2.4 scaling solution frequency with subdomain count

We test scalability to harder (higher-frequency) solutions by increasing ω_0 while simultaneously increasing J_1 (and the number of collocation points proportionally) for the baseline $L = 1$ model. This keeps the *effective resolution per subdomain* approximately constant, so that changes in performance reflect the optimisation/solve strategy rather than a trivial loss of spatial resolution. In this section, we also assess whether including multiple levels can improve scaling performance by aiding global subdomain communication with the addition of coarser levels.

Key observations

Figure 5 and Table 5 show that both the FBPINN and ELM-FBPINN converge more slowly as ω_0 increases, but ELM-FBPINN consistently achieves lower errors and

Network	(ω_0, J)	(h, K)	δ	$\kappa(M)$	Optimiser	e_{L_1}	Time (s)
FCN	(80, 2)	(1, 12)	2.9	N/A	FBPINN-Adam	$7.7\pm 0.0e-01$	9.2 ± 0.1
FCN	(80, 4)	(1, 12)	2.9	N/A	FBPINN-Adam	$7.0\pm 0.3e-01$	$1.2\pm 0.0e+01$
FCN	(80, 6)	(1, 12)	2.9	N/A	FBPINN-Adam	$5.7\pm 0.6e-01$	$1.3\pm 0.0e+01$
FCN	(80, 8)	(1, 12)	2.9	N/A	FBPINN-Adam	$4.6\pm 1.5e-01$	$1.4\pm 0.0e+01$
FCN	(80, 10)	(1, 12)	2.9	N/A	FBPINN-Adam	$2.3\pm 0.8e-01$	$1.7\pm 0.0e+01$
FCN	(80, 12)	(1, 12)	2.9	N/A	FBPINN-Adam	$1.3\pm 4.0e-02$	$1.9\pm 0.0e+01$
FCN	(80, 14)	(1, 12)	2.9	N/A	FBPINN-Adam	$8.1\pm 5.9e-03$	$2.0\pm 0.0e+01$
FCN	(80, 16)	(1, 12)	2.9	N/A	FBPINN-Adam	$2.0\pm 1.6e-03$	$2.2\pm 0.0e+01$
FCN	(80, 18)	(1, 12)	2.9	N/A	FBPINN-Adam	$1.1\pm 0.7e-03$	$2.4\pm 0.0e+01$
FCN	(80, 20)	(1, 12)	2.9	N/A	FBPINN-Adam	$1.1\pm 0.4e-03$	$3.2\pm 0.1e+01$
FCN	(80, 24)	(1, 12)	2.9	N/A	FBPINN-Adam	$2.8\pm 0.8e-03$	$3.4\pm 0.1e+01$
FCN	(80, 32)	(1, 12)	2.9	N/A	FBPINN-Adam	$6.3\pm 2.2e-03$	$4.2\pm 0.1e+01$
FCN	(80, 48)	(1, 12)	2.9	N/A	FBPINN-Adam	$9.4\pm 2.8e-03$	$6.0\pm 0.1e+01$
FCN	(80, 64)	(1, 12)	2.9	N/A	FBPINN-Adam	$8.3\pm 1.2e-03$	$7.7\pm 0.2e+01$
FCN	(80, 92)	(1, 12)	2.9	N/A	FBPINN-Adam	$4.9\pm 1.4e-03$	$1.1\pm 0.0e+02$
FCN	(80, 128)	(1, 12)	2.9	N/A	FBPINN-Adam	$1.2\pm 0.3e-02$	$1.4\pm 0.0e+02$
ELM	(80, 2)	(1, 12)	2.9	$2.8e+17$	LSQR	$7.5\pm 0.2e-01$	5.2 ± 0.1
ELM	(80, 4)	(1, 12)	2.9	$9.1e+17$	LSQR	$5.7\pm 1.4e-01$	4.5 ± 0.1
ELM	(80, 6)	(1, 12)	2.9	$2.0e+18$	LSQR	$9.9\pm 11.2e-02$	4.3 ± 0.0
ELM	(80, 8)	(1, 12)	2.9	$2.1e+18$	LSQR	$9.4\pm 3.9e-03$	4.5 ± 0.0
ELM	(80, 10)	(1, 12)	2.9	$3.8e+17$	LSQR	$9.7\pm 6.2e-04$	4.8 ± 0.0
ELM	(80, 12)	(1, 12)	2.9	$9.7e+17$	LSQR	$3.0\pm 3.0e-04$	4.6 ± 0.0
ELM	(80, 14)	(1, 12)	2.9	$8.4e+17$	LSQR	$1.7\pm 0.6e-04$	4.7 ± 0.1
ELM	(80, 16)	(1, 12)	2.9	$1.0e+18$	LSQR	$1.3\pm 0.5e-04$	4.9 ± 0.1
ELM	(80, 18)	(1, 12)	2.9	$1.8e+18$	LSQR	$1.2\pm 1.0e-04$	5.4 ± 0.2
ELM	(80, 20)	(1, 12)	2.9	$2.2e+18$	LSQR	$1.1\pm 0.6e-04$	5.5 ± 0.2
ELM	(80, 24)	(1, 12)	2.9	$3.9e+18$	LSQR	$2.0\pm 1.1e-04$	5.7 ± 0.4
ELM	(80, 32)	(1, 12)	2.9	$3.7e+18$	LSQR	$2.4\pm 3.1e-04$	6.4 ± 0.0
ELM	(80, 48)	(1, 12)	2.9	$3.2e+18$	LSQR	$4.0\pm 10.5e-05$	6.4 ± 0.1
ELM	(80, 64)	(1, 12)	2.9	$5.1e+18$	LSQR	$7.3\pm 10.9e-05$	7.1 ± 0.1
ELM	(80, 92)	(1, 12)	2.9	$3.2e+19$	LSQR	$5.7\pm 9.5e-05$	8.2 ± 0.1
ELM	(80, 128)	(1, 12)	2.9	$1.3e+19$	LSQR	$1.6\pm 0.9e-04$	9.7 ± 0.3

Table 4: Final e_{L_1} values and total run time for each model at different number of subdomains, J , for the 1D damped harmonic oscillator, where J lists the number of subdomains for each level (here, in all cases $L = 1$).

shorter run times across all tested frequencies. Moreover adding multiple levels significantly improves the accuracy of the ELM-FBPINN, with only a small increase in training time. This suggests that adding coarse levels aids global subdomain communication and facilitates faster convergence, whilst keeping the least squares system sparse and efficient to solve.

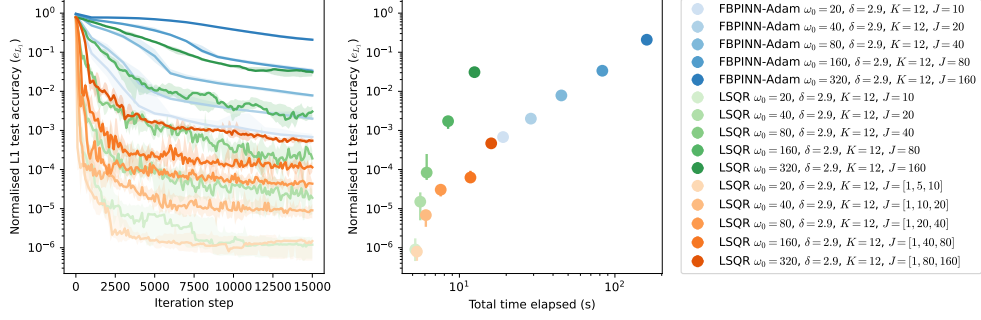


Fig. 5: All models e_{L^1} vs number of subdomains, J , and solution frequency, ω_0 , for FBPINN and multilevel ELM-FBPINN for the 1D damped harmonic oscillator, where J lists the number of subdomains for each level.

Network	(ω_0, J)	(h, K)	δ	$\kappa(M)$	Optimiser	e_{L^1}	Time (s)
FCN	(20, 10)	(1, 12)	2.9	N/A	FBPINN-Adam	$6.8 \pm 3.1e-04$	$1.9 \pm 0.1e+01$
FCN	(40, 20)	(1, 12)	2.9	N/A	FBPINN-Adam	$2.0 \pm 0.6e-03$	$2.9 \pm 0.1e+01$
FCN	(80, 40)	(1, 12)	2.9	N/A	FBPINN-Adam	$7.9 \pm 1.3e-03$	$4.5 \pm 0.0e+01$
FCN	(160, 80)	(1, 12)	2.9	N/A	FBPINN-Adam	$3.4 \pm 0.6e-02$	$8.3 \pm 0.1e+01$
FCN	(320, 160)	(1, 12)	2.9	N/A	FBPINN-Adam	$2.1 \pm 0.3e-01$	$1.6 \pm 0.1e+02$
ELM	(20, 10)	(1, 12)	2.9	$9.0e+17$	LSQR	$9.0 \pm 12.8e-07$	5.2 ± 0.1
ELM	(40, 20)	(1, 12)	2.9	$1.3e+18$	LSQR	$1.5 \pm 2.1e-05$	5.6 ± 0.1
ELM	(80, 40)	(1, 12)	2.9	$1.2e+18$	LSQR	$8.4 \pm 19.5e-05$	6.2 ± 0.1
ELM	(160, 80)	(1, 12)	2.9	$5.0e+18$	LSQR	$1.7 \pm 0.9e-03$	8.5 ± 0.2
ELM	(320, 160)	(1, 12)	2.9	$3.6e+18$	LSQR	$3.1 \pm 0.9e-02$	$1.3 \pm 0.0e+01$
ELM	(20, [1, 5, 10])	(1, 12)	2.9	$1.4e+16$	LSQR	$8.0 \pm 7.7e-07$	5.3 ± 0.0
ELM	(40, [1, 10, 20])	(1, 12)	2.9	$6.8e+14$	LSQR	$6.8 \pm 3.9e-06$	6.1 ± 0.1
ELM	(80, [1, 20, 40])	(1, 12)	2.9	$4.4e+14$	LSQR	$3.0 \pm 1.9e-05$	7.6 ± 0.1
ELM	(160, [1, 40, 80])	(1, 12)	2.9	$3.6e+14$	LSQR	$6.2 \pm 4.3e-05$	$1.2 \pm 0.0e+01$
ELM	(320, [1, 80, 160])	(1, 12)	2.9	$4.4e+14$	LSQR	$4.7 \pm 0.4e-04$	$1.6 \pm 0.0e+01$

Table 5: Final e_{L^1} values and total run time for each model at different frequency ω_0 for the 1D damped harmonic oscillator, where J lists the number of subdomains for each level.

4.2.5 Summary of 1D findings

The 1D experiments support four consistent conclusions: (i) localisation is essential on this oscillatory problem (PINN fails; decomposed methods succeed), (ii) for sufficient localisation and local width, ELM-FBPINN provides a faster route to accurate solutions than gradient-trained FBPINN, (iii) increasing J_1 expands the trial space primarily via spatially distinct degrees of freedom, whereas increasing K eventually introduces correlated features and ill-conditioning with diminishing accuracy gains, and (iv) using multilevel models with coarse levels further improves performance by aiding global subdomain communication.

4.3 2D – Multi-scale Laplace

We next evaluate all models with a 2D multi-scale Laplace problem, as defined in [8]. Compared to the 1D oscillator, this problem combines higher dimensionality with multi-frequency spatial structure, increasing both representational and optimisation difficulty.

Problem definition

The problem is given by

$$\begin{cases} -\Delta u = f, & \text{in } \Omega = [0, 1]^2, \\ u = 0, & \text{on } \partial\Omega. \end{cases} \quad (16)$$

with a source term given by

$$f(x_1, x_2) = \frac{2}{n_\omega} \sum_{i=1}^{n_\omega} (\omega_i \pi)^2 \sin(\omega_i \pi x_1) \sin(\omega_i \pi x_2). \quad (17)$$

In this case the exact solution is

$$u(x_1, x_2) = \frac{1}{n_\omega} \sum_{i=1}^{n_\omega} \sin(\omega_i \pi x_1) \sin(\omega_i \pi x_2). \quad (18)$$

We choose ω_i such that the solution is highly multi-scale, with the number of multi-scale components controlled by the parameter n_ω , and we vary n_ω and ω_i to control the problem difficulty.

Hard boundary constraints

For this problem, we use a hard-constraining approach, as originally described by [1], to assert boundary conditions. Specifically, we use the following solution ansatz

$$\tilde{u}(x_1, x_2) = \tanh(\omega_{n_\omega} x_1) \tanh(\omega_{n_\omega} (1 - x_1)) \tanh(\omega_{n_\omega} x_2) \tanh(\omega_{n_\omega} (1 - x_2)) \hat{u}(x_1, x_2). \quad (19)$$

It is straightforward to verify that this ansatz inherently satisfies the boundary condition in Equation (16). As a result, the boundary loss terms in Equation (3) can be omitted. Importantly, with this ansatz, Equation (3) remains quadratic in \mathbf{a} , ensuring that the least-squares system in Equation (4) can still be formed. We also note that the tanh terms become sharper with increasing ω_{n_ω} , which is crucial to guarantee that the effect of the constraining operator is negligible at a distance of one solution half-cycle ($1/\omega_{n_\omega}$) from the boundary.

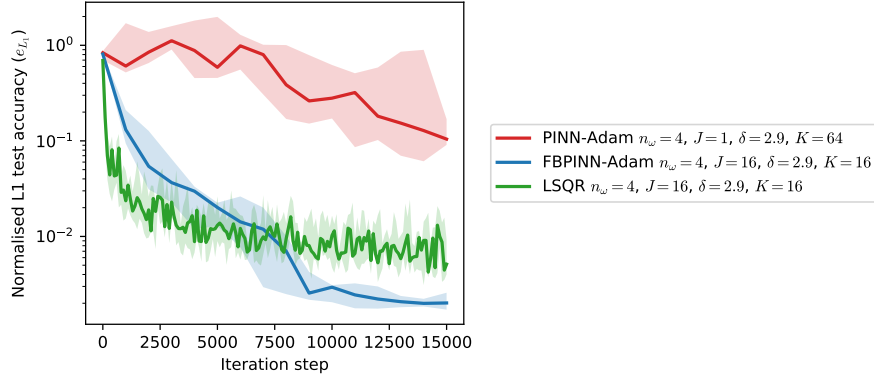


Fig. 6: Logarithm of the L^1 test error versus iteration count for the baseline 2D multi-scale Laplace problem, where J lists the number of subdomains along each input dimension for each level (here, in all cases $L = 1$).

Physics-informed objective

With the use of hard boundary constraints, the loss function reduces to

$$\mathcal{L} = \mathcal{L}_{\text{phys}} = \frac{1}{N_I} \sum_{i=1}^{N_I} (-\Delta \tilde{u} - f)^2(\mathbf{x}_i). \quad (20)$$

4.3.1 Baseline

We establish a baseline configuration. We fix $n_\omega = 4$, choosing frequency components $\omega_1 = 4$, $\omega_2 = 8$, $\omega_3 = 12$, and $\omega_4 = 16$. The resulting solution (see Figure 7) contains multiple interacting sine modes, introducing progressively finer spatial oscillations that are challenging for globally trained networks. The PINN uses $h = 2$ hidden layers with $K = 64$ basis functions per layer, matching the 1D configuration. Both the FBPINN and ELM-FBPINN use a single hidden layer ($h = 1$) with $K = 16$, and a one-level decomposition with $J_1 = 16 \times 16 = 256$ subdomains with a width ratio $\delta = 2.9$. All models use a weight scaling of $R = 1$ and are trained on $80 \times 80 = 6400$ regularly spaced collocation points and tested on $M = 96 \times 96 = 9216$ regularly spaced points.

Figure 6 shows the convergence curves. The PINN does not converge fully within the allotted budget, reflecting the difficulty of fitting multi-scale structure with a single global network trained by gradient descent. Both FBPINN and ELM-FBPINN converge to acceptable e_{L^1} values, with FBPINN achieving the lowest final error. The improvement over PINN highlights the benefit of domain localisation. ELM-FBPINN exhibits rapid initial convergence, corresponding to the early iterations of the least-squares solver efficiently reducing dominant residual components, followed by a slower phase as finer-scale interactions dominate. Table 6 reports final e_{L^1} values and wall-clock times. The PINN and FBPINN are nearly two orders of magnitude slower in runtime than the ELM-FBPINN, reflecting increased expense of nonlinear optimisation in the higher-dimensional multi-scale setting.

Network	(n_ω, J)	(h, K)	δ	$\kappa(M)$	Optimiser	e_{L_1}	Time (s)
FCN	(4, 1)	(2, 64)	2.9	N/A	PINN-Adam	$1.0 \pm 0.9e-01$	$1.6 \pm 0.0e+03$
FCN	(4, 16)	(1, 16)	2.9	N/A	FBPINN-Adam	$1.8 \pm 0.4e-03$	$2.6 \pm 0.2e+03$
ELM	(4, 16)	(1, 16)	2.9	$1.4e+09$	LSQR	$3.8 \pm 1.2e-03$	$4.2 \pm 0.0e+01$

Table 6: Baseline results for the 2D multi-scale Laplace problem, where J lists the number of subdomains along each input dimension for each level (here, in all cases $L = 1$).

We also show the model predictions in Figure 6 for the same ELM-FBPINN, but with $L = 3$ and $J = [1, 8, 16]$ subdomains, where J lists the number of subdomains along each input dimension for each level (i.e., $J_1 = 1 \times 1$, $J_2 = 8 \times 8$, and $J_3 = 16 \times 16$). The multilevel solution is visually indistinguishable from the exact solution, and recovers not only the dominant spatial oscillations but also the finer-scale components.

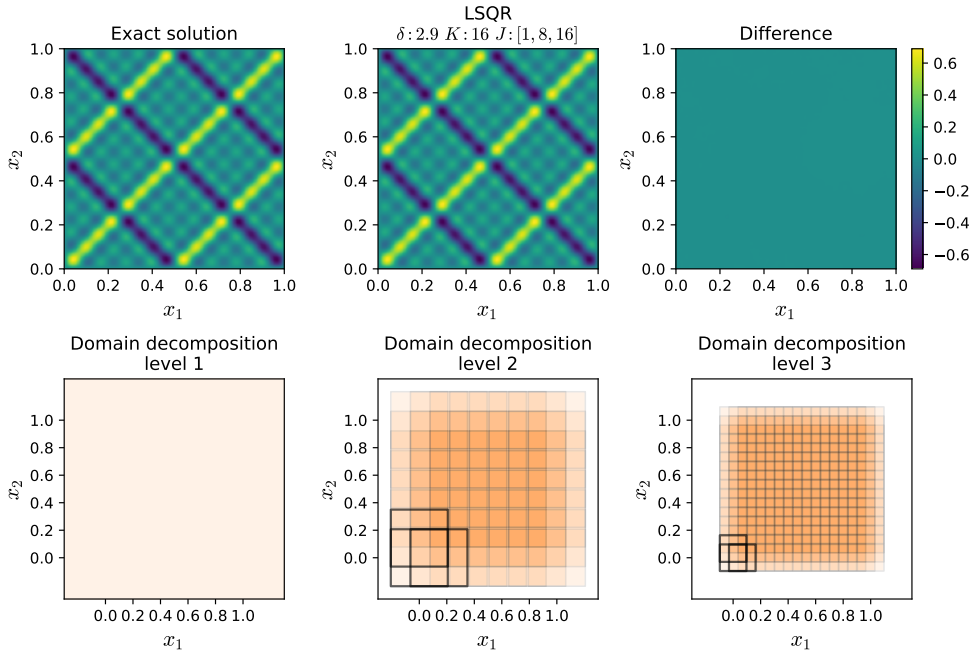


Fig. 7: Model predictions versus the exact solution for the 2D multi-scale Laplace problem with a multilevel ELM-FBPINN, where J lists the number of subdomains along each input dimension for each level; multilevel domain decomposition.

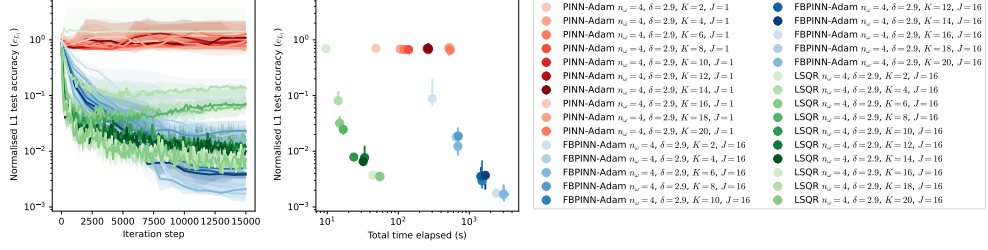


Fig. 8: All models e_{L^1} vs number of basis functions, K , for the 2D multi-scale Laplace problem, where J lists the number of subdomains along each input dimension for each level (here, in all cases $L = 1$).

4.3.2 Varying number of basis functions

We vary the number of basis functions K of the baseline $L = 1$ model to probe how each method exploits increased local capacity while keeping domain decomposition and sampling fixed. This ablation separates (i) expressivity limitations at small K from (ii) redundancy and conditioning effects at larger K .

Key observations

Figure 8 shows the convergence behaviour and Table 7 summarises the final errors and runtimes. All PINN configurations exhibit similar non-convergent trends, indicating that increasing width alone does not resolve the optimisation difficulty associated with multi-scale structure in a single global network. Both decomposed methods converge for moderate K . FBPINN improves steadily as K increases and achieves the lowest final errors, demonstrating that additional trainable local basis functions enhance expressivity in the 2D multi-scale setting. ELM-FBPINN also improves with increasing K , although very small values ($K = 2, 4$) lead to instability or large variance due to insufficient capacity and sensitivity to random feature alignment. ELM-FBPINN consistently exhibits faster initial convergence than FBPINN, reflecting the efficiency of solving a single least-squares problem for the dominant coefficients. For moderate to large K , its final errors remain within approximately one order of magnitude of FBPINN while requiring nearly two orders of magnitude less wall-clock time, highlighting a precision–efficiency trade-off.

Interpretation

In the low-capacity regime, both decomposed methods are limited by insufficient local expressivity, with ELM-FBPINN particularly sensitive to random feature alignment. As K increases, accuracy improves until diminishing returns appear. The persistent failure of PINN across all K confirms that width alone does not compensate for optimisation difficulty in multi-scale, two-dimensional problems. Overall, FBPINN benefits from the flexibility of trainable hidden weights, whereas ELM-FBPINN offers competitive accuracy at significantly reduced computational cost.

Network	(n_ω, J)	(h, K)	δ	$\kappa(M)$	Optimiser	e_{L_1}	Time (s)
FCN	(4, 1)	(2, 2)	2.9	N/A	PINN-Adam	$7.0 \pm 0.3e-01$	$4.8 \pm 0.1e+01$
FCN	(4, 1)	(2, 4)	2.9	N/A	PINN-Adam	$6.8 \pm 0.8e-01$	$1.1 \pm 0.0e+02$
FCN	(4, 1)	(2, 6)	2.9	N/A	PINN-Adam	$6.7 \pm 0.5e-01$	$1.2 \pm 0.0e+02$
FCN	(4, 1)	(2, 8)	2.9	N/A	PINN-Adam	$6.7 \pm 0.8e-01$	$1.4 \pm 0.0e+02$
FCN	(4, 1)	(2, 10)	2.9	N/A	PINN-Adam	$6.7 \pm 1.2e-01$	$2.6 \pm 0.0e+02$
FCN	(4, 1)	(2, 12)	2.9	N/A	PINN-Adam	$7.0 \pm 1.2e-01$	$2.6 \pm 0.1e+02$
FCN	(4, 1)	(2, 14)	2.9	N/A	PINN-Adam	$7.0 \pm 2.2e-01$	$2.7 \pm 0.1e+02$
FCN	(4, 1)	(2, 16)	2.9	N/A	PINN-Adam	$7.4 \pm 1.5e-01$	$5.3 \pm 0.2e+02$
FCN	(4, 1)	(2, 18)	2.9	N/A	PINN-Adam	$7.1 \pm 2.1e-01$	$5.2 \pm 0.1e+02$
FCN	(4, 1)	(2, 20)	2.9	N/A	PINN-Adam	$6.6 \pm 2.4e-01$	$5.4 \pm 0.0e+02$
FCN	(4, 16)	(1, 2)	2.9	N/A	FBPINN-Adam	$8.8 \pm 13.2e-02$	$3.0 \pm 0.1e+02$
FCN	(4, 16)	(1, 4)	2.9	N/A	FBPINN-Adam	$1.8 \pm 1.2e-02$	$6.5 \pm 0.1e+02$
FCN	(4, 16)	(1, 6)	2.9	N/A	FBPINN-Adam	$1.2 \pm 1.8e-02$	$6.9 \pm 0.1e+02$
FCN	(4, 16)	(1, 8)	2.9	N/A	FBPINN-Adam	$1.9 \pm 1.1e-02$	$7.0 \pm 0.1e+02$
FCN	(4, 16)	(1, 10)	2.9	N/A	FBPINN-Adam	$2.9 \pm 4.7e-03$	$1.5 \pm 0.0e+03$
FCN	(4, 16)	(1, 12)	2.9	N/A	FBPINN-Adam	$3.5 \pm 2.5e-03$	$1.5 \pm 0.0e+03$
FCN	(4, 16)	(1, 14)	2.9	N/A	FBPINN-Adam	$3.7 \pm 1.8e-03$	$1.7 \pm 0.1e+03$
FCN	(4, 16)	(1, 16)	2.9	N/A	FBPINN-Adam	$1.8 \pm 0.4e-03$	$2.4 \pm 0.0e+03$
FCN	(4, 16)	(1, 18)	2.9	N/A	FBPINN-Adam	$1.7 \pm 1.2e-03$	$3.0 \pm 0.4e+03$
FCN	(4, 16)	(1, 20)	2.9	N/A	FBPINN-Adam	$1.7 \pm 1.2e-03$	$3.1 \pm 0.4e+03$
ELM	(4, 16)	(1, 2)	2.9	$1.9e+03$	LSQR	$6.9 \pm 0.0e-01$	9.6 ± 0.2
ELM	(4, 16)	(1, 4)	2.9	$5.6e+04$	LSQR	$8.1 \pm 4.6e-02$	$1.4 \pm 0.1e+01$
ELM	(4, 16)	(1, 6)	2.9	$1.1e+06$	LSQR	$3.2 \pm 1.6e-02$	$1.5 \pm 0.0e+01$
ELM	(4, 16)	(1, 8)	2.9	$5.1e+17$	LSQR	$2.5 \pm 0.8e-02$	$1.7 \pm 0.0e+01$
ELM	(4, 16)	(1, 10)	2.9	$5.3e+07$	LSQR	$7.9 \pm 2.1e-03$	$2.4 \pm 0.2e+01$
ELM	(4, 16)	(1, 12)	2.9	$5.9e+08$	LSQR	$7.7 \pm 5.5e-03$	$3.4 \pm 0.2e+01$
ELM	(4, 16)	(1, 14)	2.9	$2.5e+10$	LSQR	$6.5 \pm 0.9e-03$	$3.2 \pm 0.1e+01$
ELM	(4, 16)	(1, 16)	2.9	$1.4e+09$	LSQR	$3.8 \pm 1.2e-03$	$4.4 \pm 0.0e+01$
ELM	(4, 16)	(1, 18)	2.9	$1.6e+10$	LSQR	$3.5 \pm 0.7e-03$	$5.5 \pm 0.0e+01$
ELM	(4, 16)	(1, 20)	2.9	$1.6e+11$	LSQR	$3.6 \pm 0.9e-03$	$5.5 \pm 0.1e+01$

Table 7: Final e_{L^1} values and total run time for each model at different number of basis functions, K , for the 2D multi-scale Laplace problem, where J lists the number of subdomains along each input dimension for each level (here, in all cases $L = 1$).

4.3.3 Varying number of subdomains

We vary the number of subdomains J_1 of the baseline $L = 1$ model while fixing all other parameters for FBPINN and ELM-FBPINN. Here we use J to denote the number of subdomains along each input dimension, i.e. $J_1 = J \times J$.

Key observations

Figure 9 shows the convergence behaviour. For small J , both methods struggle, with $J = 2$ failing for both and $J = 4$ exhibiting instability. In this regime, localisation is too coarse to isolate the multi-frequency structure of the solution. For moderate and

large J , both methods converge reliably. FBPINN consistently attains lower e_{L^1} values than ELM-FBPINN, with the gap remaining approximately one order of magnitude across most tested values. In contrast to the 1D case, increasing localisation alone is insufficient for ELM-FBPINN to match the accuracy of fully trainable subdomain networks. ELM-FBPINN exhibits faster initial convergence for $J \gtrsim 10$, reflecting the efficiency of the global least-squares solve. The subsequent slower decay phase suggests residual inter-subdomain interactions that are more difficult to capture with fixed random features. Final errors and runtimes are summarised in Table 8. While ELM-FBPINN retains a significant runtime advantage of nearly two orders of magnitude, this gain comes at the cost of reduced precision.

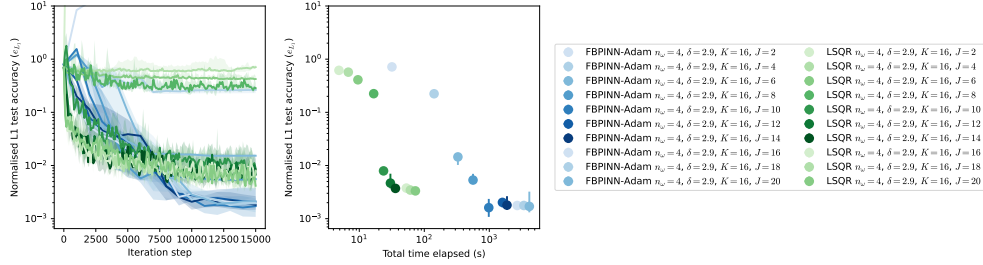


Fig. 9: All models e_{L^1} vs number of subdomains, J , for FBPINN and ELM-FBPINN, for the 2D multi-scale Laplace problem, where J lists the number of subdomains along each input dimension for each level (here, in all cases $L = 1$).

Interpretation

In the 2D multi-scale setting, localisation alone is insufficient for fixed random features to match the flexibility of trainable hidden weights. While increasing J improves accuracy for both methods, the persistent performance gap indicates that adaptivity within subdomains becomes increasingly important as spatial complexity grows. ELM-FBPINN remains computationally attractive, but its fixed feature basis limits its ability to fully capture interacting frequency components in two dimensions.

4.3.4 Scaling solution frequency with subdomains

We investigate robustness under increasing spectral complexity by varying the number of frequency components n_ω in the exact solution. Specifically, our most complex problem is defined as $n_\omega = 7$ with $\omega_i \in \{4, 8, 12, 16, 20, 24, 32\}$, $i = 1, \dots, 7$, with simpler problems defined by taking the first n_ω elements of this set. To maintain approximately constant resolution per subdomain, we scale the number of subdomains J alongside n_ω (and the number of collocation points proportionally). This isolates the effect of increasing global complexity while preserving local resolution. In this section, we also assess whether including multiple levels can improve scaling performance.

Network	(n_ω, J)	(h, K)	δ	$\kappa(M)$	Optimiser	e_{L_1}	Time (s)
FCN	(4, 2)	(1, 16)	2.9	N/A	FBPINN-Adam	$7.2 \pm 1.5e-01$	$3.2 \pm 0.0e+01$
FCN	(4, 4)	(1, 16)	2.9	N/A	FBPINN-Adam	$2.2 \pm 0.2e-01$	$1.4 \pm 0.0e+02$
FCN	(4, 6)	(1, 16)	2.9	N/A	FBPINN-Adam	$1.5 \pm 0.6e-02$	$3.3 \pm 0.0e+02$
FCN	(4, 8)	(1, 16)	2.9	N/A	FBPINN-Adam	$5.3 \pm 2.1e-03$	$5.6 \pm 0.1e+02$
FCN	(4, 10)	(1, 16)	2.9	N/A	FBPINN-Adam	$1.6 \pm 1.3e-03$	$9.8 \pm 0.2e+02$
FCN	(4, 12)	(1, 16)	2.9	N/A	FBPINN-Adam	$2.0 \pm 0.4e-03$	$1.6 \pm 0.0e+03$
FCN	(4, 14)	(1, 16)	2.9	N/A	FBPINN-Adam	$1.8 \pm 1.2e-03$	$1.9 \pm 0.0e+03$
FCN	(4, 16)	(1, 16)	2.9	N/A	FBPINN-Adam	$1.8 \pm 0.4e-03$	$2.7 \pm 0.1e+03$
FCN	(4, 18)	(1, 16)	2.9	N/A	FBPINN-Adam	$1.8 \pm 0.4e-03$	$3.4 \pm 0.0e+03$
FCN	(4, 20)	(1, 16)	2.9	N/A	FBPINN-Adam	$1.7 \pm 1.9e-03$	$4.1 \pm 0.1e+03$
ELM	(4, 2)	(1, 16)	2.9	$1.3e+10$	LSQR	$6.2 \pm 0.0e-01$	4.9 ± 0.1
ELM	(4, 4)	(1, 16)	2.9	$7.6e+08$	LSQR	$5.7 \pm 0.1e-01$	6.8 ± 0.0
ELM	(4, 6)	(1, 16)	2.9	$6.6e+08$	LSQR	$4.1 \pm 0.1e-01$	9.5 ± 0.2
ELM	(4, 8)	(1, 16)	2.9	$1.1e+09$	LSQR	$2.2 \pm 0.5e-01$	$1.7 \pm 0.0e+01$
ELM	(4, 10)	(1, 16)	2.9	$2.6e+09$	LSQR	$7.9 \pm 1.4e-03$	$2.4 \pm 0.1e+01$
ELM	(4, 12)	(1, 16)	2.9	$1.1e+09$	LSQR	$4.7 \pm 3.3e-03$	$3.0 \pm 0.2e+01$
ELM	(4, 14)	(1, 16)	2.9	$1.8e+09$	LSQR	$3.7 \pm 0.8e-03$	$3.6 \pm 0.0e+01$
ELM	(4, 16)	(1, 16)	2.9	$1.4e+09$	LSQR	$3.8 \pm 1.2e-03$	$5.3 \pm 0.2e+01$
ELM	(4, 18)	(1, 16)	2.9	$5.7e+09$	LSQR	$3.4 \pm 0.8e-03$	$6.1 \pm 0.1e+01$
ELM	(4, 20)	(1, 16)	2.9	$3.3e+09$	LSQR	$3.3 \pm 0.5e-03$	$7.3 \pm 0.2e+01$

Table 8: Final e_{L_1} values and average runtime for varying number of subdomains, J , for the 2D multi-scale Laplace problem, where J lists the number of subdomains along each input dimension for each level (here, in all cases $L = 1$).

Key observations

Figure 10 shows the convergence behaviour and Table 9 reports final errors. ELM-FBPINN and multilevel ELM-FBPINNs consistently exhibit the fastest initial convergence across all values of n_ω , reflecting the efficiency of the global least-squares solve. Although convergence curves appear visually distinct, the absolute differences in final e_{L_1} values across all models tested remain modest for most n_ω , with the multilevel ELM-FBPINN most accurate on average, particularly for the highest frequencies tested. The max–min range of the ELM-FBPINN is slightly smaller than the FBPINN, indicating marginally more uniform performance as spectral richness increases. All methods maintain stable convergence as frequency increases, with no catastrophic degradation observed.

Interpretation

All methods scale reasonably well as spectral richness increases, whilst the ELM-FBPINN and multilevel ELM-FBPINN remain nearly two orders of magnitude faster than the FBPINN; we note adaptive stopping for the least-squares solver could further reduce ELM-FBPINN cost without affecting accuracy.

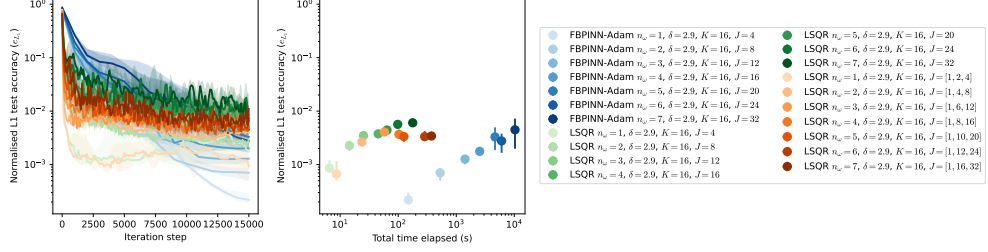


Fig. 10: All models e_{L_1} as the number of frequency components n_ω increases (with J scaled accordingly) for the 2D multi-scale Laplace problem, where J lists the number of subdomains along each input dimension for each level.

Network	(n_ω, J)	(h, K)	δ	$\kappa(M)$	Optimiser	e_{L_1}	Time (s)
FCN	(1, 4)	(1, 16)	2.9	N/A	FBPINN-Adam	$2.2 \pm 1.1e-04$	$1.5 \pm 0.1e+02$
FCN	(2, 8)	(1, 16)	2.9	N/A	FBPINN-Adam	$7.1 \pm 3.7e-04$	$5.3 \pm 0.1e+02$
FCN	(3, 12)	(1, 16)	2.9	N/A	FBPINN-Adam	$1.3 \pm 0.3e-03$	$1.4 \pm 0.0e+03$
FCN	(4, 16)	(1, 16)	2.9	N/A	FBPINN-Adam	$1.8 \pm 0.4e-03$	$2.5 \pm 0.0e+03$
FCN	(5, 20)	(1, 16)	2.9	N/A	FBPINN-Adam	$3.3 \pm 3.1e-03$	$4.6 \pm 0.0e+03$
FCN	(6, 24)	(1, 16)	2.9	N/A	FBPINN-Adam	$2.8 \pm 2.1e-03$	$6.0 \pm 0.2e+03$
FCN	(7, 32)	(1, 16)	2.9	N/A	FBPINN-Adam	$4.5 \pm 5.3e-03$	$1.0 \pm 0.0e+04$
ELM	(1, 4)	(1, 16)	2.9	$1.0e+09$	LSQR	$8.6 \pm 5.0e-04$	6.5 ± 0.1
ELM	(2, 8)	(1, 16)	2.9	$1.3e+09$	LSQR	$2.3 \pm 0.9e-03$	$1.4 \pm 0.1e+01$
ELM	(3, 12)	(1, 16)	2.9	$1.3e+09$	LSQR	$3.5 \pm 0.5e-03$	$2.5 \pm 0.0e+01$
ELM	(4, 16)	(1, 16)	2.9	$1.4e+09$	LSQR	$3.8 \pm 1.2e-03$	$4.5 \pm 0.1e+01$
ELM	(5, 20)	(1, 16)	2.9	$2.8e+09$	LSQR	$4.4 \pm 0.7e-03$	$6.4 \pm 0.0e+01$
ELM	(6, 24)	(1, 16)	2.9	$4.0e+09$	LSQR	$5.7 \pm 1.1e-03$	$9.8 \pm 0.4e+01$
ELM	(7, 32)	(1, 16)	2.9	$1.7e+09$	LSQR	$6.0 \pm 1.4e-03$	$1.8 \pm 0.1e+02$
ELM	(1, [1, 2, 4])	(1, 16)	2.9	$3.8e+16$	LSQR	$6.7 \pm 6.7e-04$	8.6 ± 0.3
ELM	(2, [1, 4, 8])	(1, 16)	2.9	$3.0e+16$	LSQR	$2.6 \pm 0.4e-03$	$2.4 \pm 0.0e+01$
ELM	(3, [1, 6, 12])	(1, 16)	2.9	$2.3e+16$	LSQR	$4.1 \pm 0.5e-03$	$5.8 \pm 0.1e+01$
ELM	(4, [1, 8, 16])	(1, 16)	2.9	$2.2e+16$	LSQR	$3.7 \pm 1.5e-03$	$1.0 \pm 0.0e+02$
ELM	(5, [1, 10, 20])	(1, 16)	2.9	$1.8e+16$	LSQR	$3.3 \pm 1.4e-03$	$1.3 \pm 0.0e+02$
ELM	(6, [1, 12, 24])	(1, 16)	2.9	$2.1e+16$	LSQR	$3.3 \pm 1.1e-03$	$2.9 \pm 0.1e+02$
ELM	(7, [1, 16, 32])	(1, 16)	2.9	$2.0e+16$	LSQR	$3.4 \pm 0.5e-03$	$3.7 \pm 0.1e+02$

Table 9: Final e_{L_1} values and average runtime for varying n_ω for the 2D multi-scale Laplace problem, where J lists the number of subdomains along each input dimension for each level.

4.3.5 Varying parameter initialisation

Finally, we vary the weight scaling parameter R in the LeCun initialisation of hidden basis function weights and biases of the baseline $L = 1$ model for both the 1D harmonic oscillator and the 2D multi-scale Laplace problem to ascertain the sensitivity of the ELM-FBPINN models to parameter initialisation.

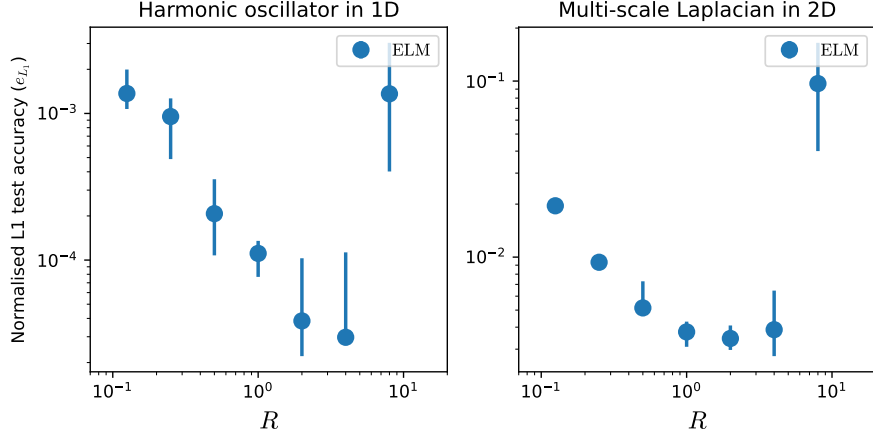


Fig. 11: Final e_{L^1} values for varying weight scaling values, R , for the 1D damped harmonic oscillator and the 2D multi-scale Laplace problems.

Key observations

Figure 11 shows that whilst the performance of ELM-FBPINN does depend on the choice of the weight scaling parameter, R , good performance is achieved for $R \in [1, 5]$ for both the 1D and 2D problems. Indeed, even for R outside this range, the accuracy obtained is typically within one order of magnitude of the optimal value, indicating robustness with respect to the choice of parameter initialisation.

5 Discussion and conclusions

We compared PINN, FBPINN, ELM-FBPINN, and multilevel ELM-FBPINN across controlled ablation studies on a 1D damped harmonic oscillator and a 2D multi-scale Laplace problem. The experiments isolated the effects of localisation (J), width (K) and spectral complexity, while measuring convergence behaviour, accuracy, conditioning, and runtime.

	PINN	FBPINN	ELM-FBPINN	Multilevel ELM-FBPINN
Multi-scale convergence	Poor	Stable	Stable (fast initial)	Stable (fast initial)
Final accuracy (1D)	Low	High	Highest	-
Final accuracy (2D)	Low	Highest	High	-
Scalability (frequency)	Poor	Stable	Stable	Stable (best accuracy)
Runtime efficiency	Slow	Moderate	Fastest	Fast

Table 10: Qualitative comparison across experiments.

Convergence behaviour

Across all configurations, ELM-FBPINN exhibits a characteristic two-phase convergence: a rapid initial reduction of error followed by slower refinement. This reflects the structure of the global least-squares solve, where dominant residual components are eliminated early. Standard PINNs fail to converge on the multi-scale configurations considered, confirming that global gradient-based training alone is insufficient for oscillatory problems.

Accuracy trade-offs

In 1D, ELM-FBPINN achieves the lowest errors in most ablations, except when activation saturation limits representational quality. In 2D, FBPINN generally attains lower final e_{L^1} values, indicating that adaptive hidden weights are advantageous when resolving interacting spatial frequencies. Nevertheless, ELM-FBPINN consistently achieves errors within the same order of magnitude while requiring substantially less computational effort.

Scalability

When frequency and model capacity are increased simultaneously, both FBPINN and ELM-FBPINN methods maintain stable error levels without catastrophic degradation. Furthermore, multilevel ELM-FBPINN perform best whilst only incurring slightly more computational cost than ELM-FBPINNs, suggesting that adding multiple coarser levels facilitates global subdomain communication and aids convergence.

Conditioning and redundancy

The ELM-FBPINN least-squares matrix \mathbf{M} typically exhibits large SVD-based condition numbers, often exceeding 10^{18} for large K . This growth is driven primarily by redundancy among randomly initialised basis functions. Increasing K introduces near-linear dependencies, while excessive localisation (J large) can also induce effective rank saturation when local solutions become simple. Despite this ill-conditioning, the least-squares solves remain sufficiently stable to produce accurate approximations, although redundancy limits further gains beyond moderate capacity.

Overall assessment

Domain decomposition is essential for multi-scale problems. Within this framework, replacing gradient-based subdomain training by a linear least-squares solve yields substantial gains in convergence speed and competitive accuracy. While fully trainable hidden representations remain advantageous in higher-dimensional settings, ELM-FBPINN offers a favourable efficiency–accuracy trade-off and demonstrates robust scalability across the tested regimes, especially when multiple levels are employed. These results position random-feature-based domain decomposition as a viable and computationally efficient alternative to gradient-trained FBPINNs for structured scientific machine learning problems.

6 Code and data availability

All code required to reproduce this work is available at <https://github.com/benmoseley/FBPINNs/tree/elm-paper/elm-paper>. All data is synthetically generated using the provided code.

References

- [1] Lagaris, I.E., Likas, A., Fotiadis, D.I.: Artificial neural networks for solving ordinary and partial differential equations. *IEEE Transactions on Neural Networks* **9**(5), 987–1000 (1998) <https://doi.org/10.1109/72.712178> arXiv:9705023 [physics]
- [2] Raissi, M., Perdikaris, P., Karniadakis, G.E.: Physics-informed neural networks: A deep learning framework for solving forward and inverse problems involving nonlinear partial differential equations. *Journal of Computational Physics* **378**, 686–707 (2019) <https://doi.org/10.1016/j.jcp.2018.10.045>
- [3] Rahaman, N., Baratin, A., Arpit, D., Draxler, F., Lin, M., Hamprecht, F.A., Bengio, Y., Courville, A.: On the spectral bias of neural networks. In: 36th International Conference on Machine Learning, ICML 2019, vol. 2019-June, pp. 9230–9239. International Machine Learning Society (IMLS), ??? (2019). <http://arxiv.org/abs/1806.08734>
- [4] Moseley, B., Markham, A., Nissen-Meyer, T.: Finite basis physics-informed neural networks (FBPINNs): a scalable domain decomposition approach for solving differential equations. *Advances in Computational Mathematics* 2023 49:4 **49**(4), 1–39 (2023) <https://doi.org/10.1007/S10444-023-10065-9>
- [5] Jagtap, A.D., Kharazmi, E., Karniadakis, G.E.: Conservative physics-informed neural networks on discrete domains for conservation laws: Applications to forward and inverse problems. *Computer Methods in Applied Mechanics and Engineering* **365**, 113028 (2020)
- [6] Jagtap, A.D., Karniadakis, G.E.: Extended physics-informed neural networks (XPINNs): A generalized space-time domain decomposition based deep learning framework for nonlinear partial differential equations. *Communications in Computational Physics* **28**(5) (2020)
- [7] Dolean, V., Heinlein, A., Mishra, S., Moseley, B.: Finite basis physics-informed neural networks as a Schwarz domain decomposition method. In: International Conference on Domain Decomposition Methods, pp. 165–172 (2022). Springer
- [8] Dolean, V., Heinlein, A., Mishra, S., Moseley, B.: Multilevel domain decomposition-based architectures for physics-informed neural networks. *Computer Methods in Applied Mechanics and Engineering* **429**, 117116 (2024)

- [9] Huang, G.B., Zhu, Q.Y., Siew, C.K.: Extreme learning machine: Theory and applications. *Neurocomputing* **70**(1-3), 489–501 (2006) <https://doi.org/10.1016/j.neucom.2005.12.126>
- [10] Chen, J., Chi, X., E, W., Yang, Z.: Bridging traditional and machine learning-based algorithms for solving pdes: the random feature method. *J Mach Learn* **1**, 268–98 (2022)
- [11] Pao, Y.-H., Takefuji, Y.: Functional-link net computing: theory, system architecture, and functionalities. *Computer* **25**(5), 76–79 (1992)
- [12] Lukoševičius, M., Jaeger, H.: Reservoir computing approaches to recurrent neural network training. *Computer Science Review* **3**(3), 127–149 (2009) <https://doi.org/10.1016/j.cosrev.2009.03.005>
- [13] Dong, S., Li, Z.: Local extreme learning machines and domain decomposition for solving linear and nonlinear partial differential equations. *Computer Methods in Applied Mechanics and Engineering* **387**, 114129 (2021) <https://doi.org/10.1016/j.cma.2021.114129>
- [14] Dwivedi, V., Parashar, N., Srinivasan, B.: Distributed learning machines for solving forward and inverse problems in partial differential equations. *Neurocomputing* **420**, 299–316 (2021) <https://doi.org/10.1016/j.neucom.2020.09.006>
- [15] Schiassi, E., Furfaro, R., Leake, C., De Florio, M., Johnston, H., Mortari, D.: Extreme theory of functional connections: A fast physics-informed neural network method for solving ordinary and partial differential equations. *Neurocomputing* **457**, 334–356 (2021) <https://doi.org/10.1016/j.neucom.2021.06.015>
- [16] Anderson, S., Dolean, V., Moseley, B., Pestana, J.: ELM-FBPINN: efficient finite-basis physics-informed neural networks (2024). <http://arxiv.org/abs/2409.01949>
- [17] Datar, C., Kapoor, T., Chandra, A., Sun, Q., Burak, I., Bolager, E.L., Veselovska, A., Fornasier, M., Dietrich, F.: Solving partial differential equations with sampled neural networks (2024). <https://arxiv.org/abs/2405.20836>
- [18] Yıldız, E., Datar, C., Rahma, A., Dolean, V., Dietrich, F.: Fast multiscale pde solvers via multilevel domain decomposition and random features. In: *ICLR 2026 Workshop on AI for PDEs* (2026). <https://openreview.net/forum?id=wA6SsMmftX>
- [19] Datar, C., Kapoor, T., Chandra, A., Sun, Q., Bolager, E.L., Burak, I., Veselovska, A., Fornasier, M., Dietrich, F.: Frozen-pinn: Fast training of accurate physics-informed neural networks with temporal causality. In: *International Conference on Learning Representations (ICLR)* (2026). *ICLR 2026 Oral*. <https://openreview.net/forum?id=3VdSuh3sie>

- [20] Shang, Y., Heinlein, A., Mishra, S., Wang, F.: Overlapping schwarz preconditioners for randomized neural networks with domain decomposition. *Computer Methods in Applied Mechanics and Engineering* **442**(1) (2025) <https://doi.org/10.1016/j.cma.2025.118011>
- [21] Beek, J.W., Dolean, V., Moseley, B.: Local feature filtering for scalable and well-conditioned domain-decomposed random feature methods. *Computer Methods in Applied Mechanics and Engineering* **449**, 118583 (2026) <https://doi.org/10.1016/j.cma.2025.118583>
- [22] LeCun, Y., Bottou, L., Orr, G., Muller, K.: Efficient BackProp. In: Orr, G., K. M. (eds.) *Neural Networks: Tricks of the Trade*. Springer, ??? (1998)
- [23] Virtanen, P., Gommers, R., Oliphant, T.E., Haberland, M., Reddy, T., Cournapeau, D., Burovski, E., Peterson, P., Weckesser, W., Bright, J., Walt, S.J., Brett, M., Wilson, J., Millman, K.J., Mayorov, N., Nelson, A.R.J., Jones, E., Kern, R., Larson, E., Carey, C.J., Polat, I., Feng, Y., Moore, E.W., VanderPlas, J., Laxalde, D., Perktold, J., Cimrman, R., Henriksen, I., Quintero, E.A., Harris, C.R., Archibald, A.M., Ribeiro, A.H., Pedregosa, F., Mulbregt, P.: SciPy 1.0: fundamental algorithms for scientific computing in Python. *Nature Methods* **17**(3), 261–272 (2020) <https://doi.org/10.1038/s41592-019-0686-2> . Accessed 2026-01-19
- [24] Bradbury, J., Frostig, R., Hawkins, P., Johnson, M.J., Leary, C., Maclaurin, D., Necula, G., Paszke, A., VanderPlas, J., Wanderman-Milne, S., Zhang, Q.: JAX: composable transformations of Python+NumPy programs (2018). <http://github.com/google/jax>
- [25] Virtanen, P., Gommers, R., Oliphant, T.E., Haberland, M., Reddy, T., Cournapeau, D., Burovski, E., Peterson, P., Weckesser, W., Bright, J., van der Walt, S.J., Brett, M., Wilson, J., Millman, K.J., Mayorov, N., Nelson, A.R.J., Jones, E., Kern, R., Larson, E., Carey, C.J., Polat, I., Feng, Y., Moore, E.W., VanderPlas, J., Laxalde, D., Perktold, J., Cimrman, R., Henriksen, I., Quintero, E.A., Harris, C.R., Archibald, A.M., Ribeiro, A.H., Pedregosa, F., van Mulbregt, P., SciPy 1.0 Contributors: SciPy 1.0: Fundamental Algorithms for Scientific Computing in Python. *Nature Methods* **17**, 261–272 (2020) <https://doi.org/10.1038/s41592-019-0686-2>